Structural Optimization of an Optical 90 Degree Hybrid Based on a Weakly-guided 4×4 Multimode Interference Coupler Using a Parallelized Real-coded Micro-genetic Algorithm

Takashi Yasui, Jun-ichiro Sugisaka, and Koichi Hirayama

Faculty of Engineering
Kitami Institute of Technology, Kitami-shi, Hokkaido, 090-8507, Japan
yasui@mail.kitami-it.ac.jp, sugisaka@mail.kitami-it.ac.jp, hirakc@mail.kitami-it.ac.jp

Abstract ─ The optimal design of a 4×4 multimode interference (MMI) coupler as an optical 90° hybrid based on a weakly-guided optical waveguide was considered. Seven geometrical parameters of a 4×4 MMI coupler were optimized by a real-coded micro-genetic algorithm, and parallelized using a message-passing interface. The beam-propagation method was used to evaluate the fitness of the MMI coupler in the optimization process. The optimized 4×4 MMI coupler showed a common-mode rejection ratio greater than 28.9 dBe and a phase error less than 2.52° across a wavelength range of 1520 to 1580 nm, which satisfied typical system requirements. The optimization process was executed on a Beowulf-style cluster comprising five identical PCs, and its parallel efficiency was 0.78.

Index Terms ─ Beam-propagation method, finite element method, genetic algorithm, multimode interference coupler, optical waveguides, parallel computation.

I. INTRODUCTION

The optical 90° hybrid is a key component for demodulating optical signals in coherent transmission systems, and is considered to be a promising candidate for next-generation high-capacity optical transmission systems. Although some configurations for the waveguide-based 90° hybrids have been proposed [1,2] for photonic integrated circuits (PICs), those based on 4×4 multimode interference (MMI) couplers have attracted considerable attention because of their simple and compact structures [3,4,5]. These MMI-based 90º hybrids are based on high-index-contrast technologies such as silicon-on-insulator (SOI) [3,4] and InP [5] waveguides.

Silica is another attractive material for PICs because of its extremely low propagation loss, low coupling loss to single-mode fibers, and low polarization dependence, and is widely used in PICs. In general, the self-imaging theory [6], which relies on a parabolic distribution of effective indices of eigenmodes in the MMI section, is used to design MMI couplers. However, it is difficult to design accurate and high-performance MMI couplers based on weakly-guided waveguides, such as silica-based waveguides using the self-imaging theory is difficult. This is because that the parabolic distribution of the effective indices of eigenmodes in the MMI section cannot be assumed in weakly guided waveguides.

To realize high-performance MMI couplers based on weakly guided waveguides, structural optimization of MMI couplers using genetic algorithms (GAs) has been considered [7,8,9]. Wang et al. [7], and West and Honkanen [8] performed structural optimization of weakly-guided MMI couplers operating at a single wavelength. In their work, a simple GA and a mode propagation analysis were employed for the optimization and propagation analysis of optical waves, respectively. Yasui et al. [9] demonstrated the structural optimization of silica-based 2×2 MMI couplers operating at wavelengths ranging from 1520 to 1580 nm, which includes the C-band of optical transmission systems. A real-coded micro-GA, which is a combination of a real-coded GA and a micro-GA (μGA), was employed for the structural optimization, and the two-dimensional beam-propagation method (BPM) based on the finite element method (FE-BPM) [10,11] was used for the propagation analysis. The BPM analysis, which is a more accurate but time-consuming method, was executed 750 times for one optimization process.

In this study, we propose a parallelized optimization method based on a real-coded μGA. Two-dimensional FE-BPM was applied to the optimization of silica-based 4×4 MMI couplers as an optical 90º hybrid to satisfy typical system requirements [4,5]. A 4×4 MMI coupler optimized by the proposed method has a common-mode rejection ratio (CMRR) greater than 28.9 dBe and a phase error less than 2.52° across a wavelength range of 1520 to 1580 nm, which satisfies the system requirements. In addition, the excess loss remained less than 0.68 dB. The optimization process was executed on a Beowulf-style cluster [12], which comprised five identical PCs,

Submitted On: January 20, 2021
Accepted On: April 30, 2021
https://doi.org/10.47037/2020.ACES.J.360506

and its parallel efficiency was 0.78.

II. NUMERICAL METHODS

A. Parallelized μ GA

A μGA is a GA with a small population, (typically five), and reinitialization. It starts with a randomly generated population. The production of individuals in the next generation by a genetic operation is performed until nominal convergence is reached. Subsequently, a new population is generated by transferring the best individual in the converged population to the new one, followed by randomly generating the remaining individuals [9,13,14].

The flowchart of the proposed algorithm parallelized with the message passing interface (MPI) [15,16] is shown in Fig. 1. Let N_p be the population number, which is equal to the number of MPI processes. First, an initial random population is generated in process 0. The genes in the population are broadcast to all the processes. Second, in the *i*-th process, a BPM analysis is executed for a 4×4 MMI coupler represented by the *i*-th individual in the population, and its fitness is evaluated. Here, the two-dimensional FE-BPM [10,11] is utilized to an equivalent two-dimensional 4×4 MMI coupler obtained by the effective index method. After a barrier synchronization to ensure that all the processes have reached the same point in the code, all fitness values were gathered to process 0. Third, if a termination condition is satisfied then the optimization process is completed; otherwise, genes in the next generation are generated. Here, the individual with the largest fitness is carried to the next generation as the elite (elitist strategy). If nominal convergence is reached, the remaining $N_p - 1$ individuals in the next generation are randomly generated; otherwise, the remaining $N_p - 1$ individuals are produced by selection and crossover. The second and third procedures are repeated until the termination condition is satisfied.

B. Real-coded GA

In a real-coded GA, a chromosome is represented as a vector of floating-point numbers, in which the elements denote the values of the parameters to be optimized [17,18]. In this study, we denote the chromosome of the *i*th individual in the *g*th generation as:

$$x^{(g,i)} = (x_1^{(g,i)}, x_2^{(g,i)}, \ldots, x_N^{(g,i)}), \tag{1}$$

where *N* is the size of the chromosome.

For the selection and crossover, a binary tournament selection and the BLX-α strategy [9,17] were applied, respectively.

C. A brief review of FE-BPM

Herein, we briefly review the FE-BPM [10, 11]. We consider an optical wave propagating in the $+z$-direction in a two-dimensional planar optical waveguide uniform in the x-direction. From Maxwell's equations, we obtain the following wave equation:

$$\frac{\partial}{\partial y}\left(p\frac{\partial \Phi}{\partial y}\right) + \frac{\partial}{\partial z}\left(p\frac{\partial \Phi}{\partial z}\right) + k_0^2 q\Phi = 0, \tag{2}$$

where $\Phi = E_x$, $p = 1$, $q = n^2$ for the transverse electric (TE) modes, and $\Phi = H_x$, $p = 1/n^2$, $q = 1$ for the transverse magnetic (TM) modes, and n is the refractive index. Substituting the solution of the form:

$$\Phi(y,z) = \varphi(y,z)\exp(-jk_0 n_0 z), \tag{3}$$

into Eq. (2), we obtain the following equation for the slowly varying complex amplitude φ:

$$p\frac{\partial^2 \varphi}{\partial z^2} - 2jk_0 n_0 p\frac{\partial \varphi}{\partial z} + \frac{\partial}{\partial y}\left(p\frac{\partial \varphi}{\partial y}\right) + k_0^2(q - n_0^2 p)\varphi = 0. \tag{4}$$

Applying the finite-element method to the cross-section of the waveguide in the y-direction of Eq. (4), we obtain:

$$[M]\frac{d^2\{\varphi\}}{dz^2} - 2jk_0 n_0[M]\frac{d\{\varphi\}}{dz} + ([K] - k_0^2 n_0^2[M])\{\varphi\} = \{0\}, \tag{5}$$

where $\{\varphi\}$ is the global electric or magnetic field vector, and $[K]$ and $[M]$ are the finite-element matrices. Applying the Crank-Nicholson algorithm for the z-direction after introducing the Padé approximation [19] and the transparent boundary condition [20] to Eq. (5), we finally obtain the following fundamental equation of the BPM:

$$[A]_i\{\varphi\}_{i+1} = [B]_i\{\varphi\}_i, \tag{6}$$

where $[A]_i$ and $[B]_i$ are the beam-propagation matrices, and the subscripts i and $i+1$ denote the quantities related to the ith and $(i+1)$th propagation steps at $z = i\Delta z$ and $(i+1)\Delta z$, respectively, and Δz is the propagation step size. When an incident field $\{\varphi\}_0$ is given, the propagating field can be calculated by solving Eq. (6).

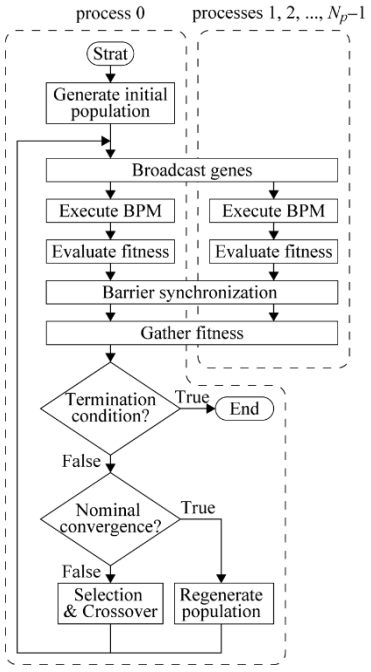

Fig. 1. Flow chart of the proposed parallelized μGA.

III. NUMERICAL MODEL

Figure 2 (a) shows a three-dimensional model of an optical 90º hybrid based on a 4×4 MMI coupler, whose core and cladding materials are ZrO_2-doped silica and silica, respectively. Let W and L be the width and length of the MMI section, respectively. The MMI has four input waveguides labeled $1, \ldots, 4$ and four output waveguides labeled $5, \ldots, 8$. We note that input waveguides 2 and 4 are not used for optical 90º hybrids [3]. The widths of the input and output waveguides were identical and equal to w. The positions of the centers of these waveguides are y_i $(i = 1, \ldots, 8)$. In addition, we assume $y_i = y_{i+4}$ for $i = 1, \ldots, 4$.

Figure 2 (b) shows an equivalent two-dimensional model, which is obtained using the effective index method, of a 4×4 MMI coupler. In this model, the refractive index of the core region is expressed as the effective index of a three-layer slab waveguide. The BPM analyses in the proposed method were performed for two-dimensional equivalent models.

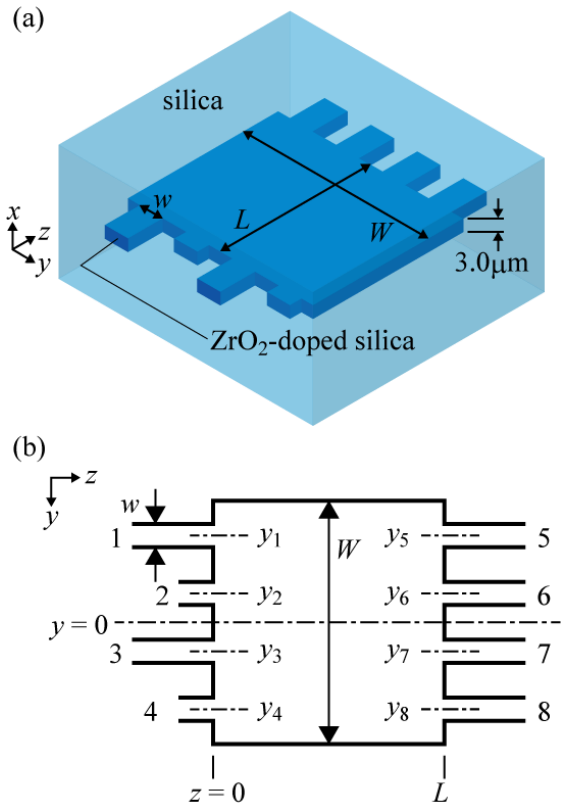

Fig. 2. Schematic structure of 4×4 MMI coupler for: (a) a three-dimensional model, and (b) an equivalent two-dimensional model.

The length of the MMI, L, and the positions of the input waveguides, y_i $(i = 1, \ldots, 4)$, are, respectively, given as follows:

$$L = \frac{3L_\pi}{4} + \Delta L, \tag{7}$$

and

$$y_i = \frac{2i - 5}{8} W + \Delta y_i, \tag{8}$$

where ΔL and Δy_i are the deviations of the length of the MMI and the positions of the center of the input waveguides, respectively. Here, L_π is the beat length in the MMI and is given by:

$$L_\pi = \frac{\pi}{\beta_0 - \beta_1}, \tag{9}$$

where β_0 and β_1 denote the propagation constants of the fundamental and first-order modes of the MMI, respectively [6].

To evaluate the fitness of a 4×4 MMI coupler, we define two properties of the coupler as follows: Let $I = \{1,3\}$, $O = \{5,6,7,8\}$, and Λ be sets of the input ports, output ports, and wavelengths for BPM analysis, respectively. Let $S_{ji}(\lambda)$ be the scattering parameter at $j \in O$ for the input from $i \in I$ at wavelength $\lambda \in \Lambda$. We define the imbalance $I_{B,i}(\lambda)$, and excess loss $X_{L,i}(\lambda)$ by the following equations, respectively:

$$I_{B,i}(\lambda) = -10 \log_{10} \left[\frac{\min \{ |S_{ji}(\lambda)|^2 | j \in O \}}{\max \{ |S_{ji}(\lambda)|^2 | j \in O \}} \right] \text{[dB]}, \tag{10}$$

and

$$X_{L,i}(\lambda) = -10 \log_{10} \left[\frac{\sum_{j \in O} |S_{ji}(\lambda)|^2}{P_{in}(\lambda)} \right] \text{[dB]}, \tag{11}$$

where $P_{in}(\lambda)$ denotes the input power. The fitness of a 4×4 MMI coupler expressed as an individual is evaluated as follows:

$$F = \exp \left\{ -\frac{1}{|I||\Lambda|} \times \sum_{i \in I} \sum_{\lambda \in \Lambda} [C_{IB} I_{B,i}(\lambda) + C_{XL} X_{L,i}(\lambda)] \right\}, \tag{12}$$

where $|I|$ and $|\Lambda|$ denote the number of elements in the sets I and Λ, respectively, and C_{IB} and C_{XL} are the weighting coefficients that determine the relative importance of $I_{B,i}(\lambda)$ and $X_{L,i}(\lambda)$, respectively.

IV. NUMERICAL RESULTS

We consider silica-based 4×4 MMI couplers as optical 90º hybrids. The operating wavelength ranged from 1520 to 1580 nm. The relative refractive index difference Δ, was 5.5% [21]. The wavelength-dependent refractive index of the cladding is given by the Sellmeier equation [22]: the thickness of the core was assumed to be 3.0 μm. The equivalent two-dimensional models obtained by the effective index method were analyzed using the BPM. The incident wave was assumed to be the TE-polarized fundamental mode of the input waveguides. The set of wavelengths used to evaluate the

fitness was $\Lambda = \{1520, 1550, 1580\ \text{nm}\}$. The values of β_0 and β_1 for Eq. (9) were evaluated at 1550 nm. The termination condition of the proposed GA was g = 50. The genes in a chromosome, which represent a 4×4 MMI coupler, and their search ranges are shown in Table 1. The coefficients in Eq. (12) are assumed as $C_{IB} = 1$ and $C_{XL} = 0.5$.

Table 1: Genes and their search ranges

j	$x_j^{(g,i)}$	$x_{j,min}$	$x_{j,max}$
1	W	20 μm	40 μm
2	ΔL	−10 μm	10 μm
3	w	2.3 μm	3.3 μm
4	Δy_1	−1 μm	1 μm
5	Δy_2	−1 μm	1 μm
6	Δy_3	−1 μm	1 μm
7	Δy_4	−1 μm	1 μm

The optimization processes were executed on a Beowulf-style cluster [12] comprise five identical PCs. Each PC had an Intel Core i7-8700 processor and a solid-state disk. The code for the proposed optimization was primarily developed in Python language with mpi4py [15], which is a Python library for MPI. From the Python code, a Fortran90 code for the BPM was executed on each process as a subprocess. The population of the GA N_p was assumed as 5; thus, each single process in Fig. 1 was assigned to one PC each.

The performance of an optical 90° hybrid is often quantified in terms of the CMRR and phase error. The CMRRs for the in-phase (I) and quadrature (Q) channels are, respectively, defined as:

$$\text{CMRR}_{I,i}(\lambda) = -20\log_{10}\left[\frac{||S_{5i}(\lambda)|^2 - |S_{8i}(\lambda)|^2|}{|S_{5i}(\lambda)|^2 + |S_{8i}(\lambda)|^2}\right]\text{[dBe]}, \quad (13)$$

and

$$\text{CMRR}_{Q,i}(\lambda) = -20\log_{10}\left[\frac{||S_{6i}(\lambda)|^2 - |S_{7i}(\lambda)|^2|}{|S_{6i}(\lambda)|^2 + |S_{7i}(\lambda)|^2}\right]\text{[dBe]}, \quad (14)$$

for the input from $i \in I$[4]. The phase error at the output port $j \in O$ with respect to output port 5 is defined as:

$$\Delta\varphi_j(\lambda) = \varphi_j(\lambda) - \varphi_5(\lambda) - (\tilde{\varphi}_j - \tilde{\varphi}_5). \quad (15)$$

Here, $\varphi_j(\lambda) = \angle S_{j3}(\lambda) - \angle S_{j1}(\lambda)$, and $\tilde{\varphi}_j$ (j = 5, ...,8) are the theoretical values of $\varphi_j(\lambda)$; in other words, $\tilde{\varphi}_5 = -45^\circ$, $\tilde{\varphi}_6 = 225^\circ$, $\tilde{\varphi}_7 = 45^\circ$, and $\tilde{\varphi}_8 = 135^\circ$ [3]. The typical system requirements of these values were CMRR ≥ 20 dBe and $|\Delta\varphi_j| \leq 5^\circ$ [4,5].

Figure 3 shows the characteristics of an optimized 4×4 MMI coupler obtained through trials, and the optimized parameters are summarized in Table 2. A CMRR greater than 28.9 dBe and a phase error less than 2.52° across the operation wavelength range, which satisfied the system requirements, were achieved. In addition, the excess loss remained less than 0.68 dB. Figure 4 shows the field distributions at the end of the 4×4 MMI coupler at wavelengths of 1520, 1550, and 1580 nm. A uniform field distribution among the output ports was realized, and thus, good values of CMRR were achieved. Conversely, we observed larger field distributions between two adjacent output waveguides, especially at wavelengths of 1520 and 1580 nm. This caused a larger excess loss at the shorter and longer sides of the operation wavelength range, as shown in Fig. 3 (c).

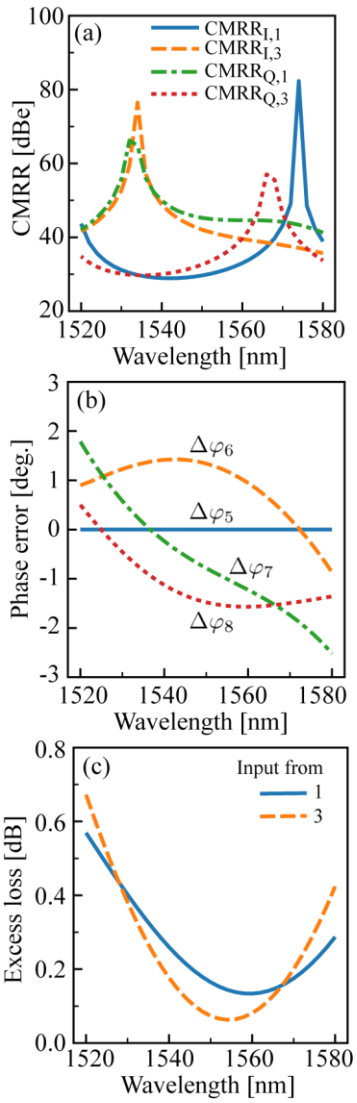

Fig. 3. Performance of an optimized 4×4 MMI coupler as an optical 90° hybrid: (a) CMRR, (b) phase error, and (c) excess loss.

The computational time of the optimization executed in parallel with five PCs was 330 s. Contrastingly, the total computational time of the BPMs in serial execution for all the individuals generated in the optimization

process was 1287 s. The speedup and parallel efficiency were 3.90, and 0.78, respectively. Here, the speedup is the ratio of the sequential to parallel execution times, and the parallel efficiency is equal to the speedup divided by the number of processes. The speedup or parallel efficiency was degraded by unbalanced computational loads in the BPM analyses, executed in parallel. This imbalance occurred, because the number of unknowns and propagation steps in the BPM analyses depended on the generated individuals in the optimization process.

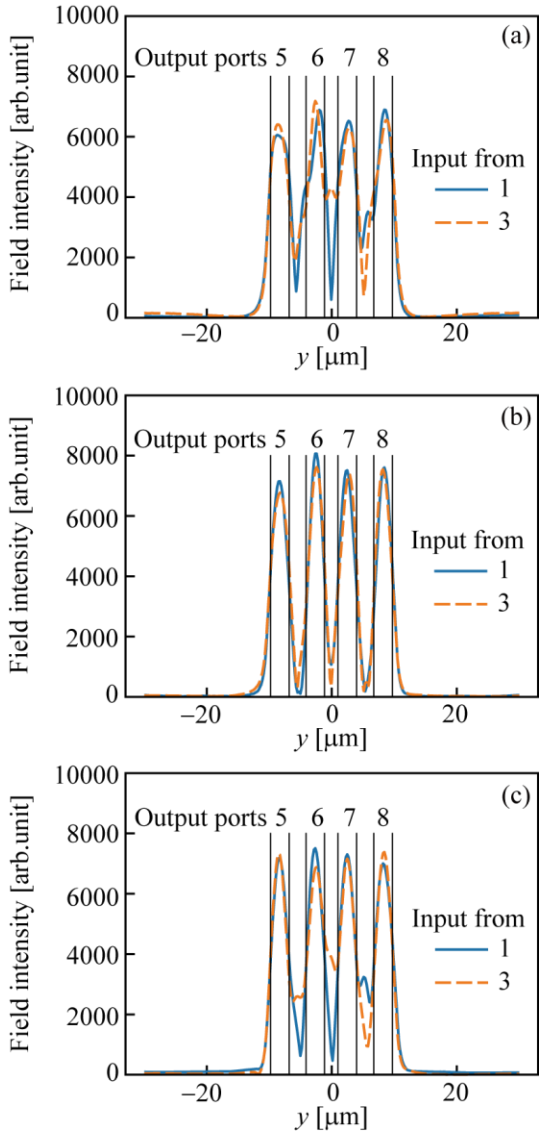

Fig. 4. Field distributions at the end of the optimized 4×4 MMI coupler at wavelengths of: (a) 1520, (b) 1550, and (c) 1580 nm. The boundaries of the output waveguides are also shown by thin solid lines.

Because of using the real-coded GA was used, the optimized structural parameters shown in Table 2 were more accurate than the typical fabrication tolerances, which were of the order of 0.1 μm for silica waveguides. To verify the influence of the fabrication tolerances on the optimized 4×4 MMI coupler, we subsequently carried out an FE-BPM analysis for a 4×4 MMI coupler having the parameters of the fabrication tolerance shown in Table 3. The results are shown in Table 4 and compared with those for the optimized model. Moreover, this model satisfies the typical system requirements of the CMRR and phase error. The excess loss is comparable to that of the optimized structure. We can see that the accuracy of the fabrication tolerance did not degrade the performance of the optimized device.

Table 2: The optimized structural parameters

Parameter	Value [μm]
W	20.606524
L	459
w	2.982606
y_1	−8.310509
y_2	−2.643767
y_3	2.471436
y_4	8.202657

Table 3: Structural parameters with the accuracy of fabrication tolerance

Parameter	Value [μm]
W	20.6
L	459
w	3.0
y_1	−8.3
y_2	−2.6
y_3	2.5
y_4	8.2

Table 4: Comparison of performance

Structural Parameters	Table 3	Table 2
CMRR [dBe]	≥ 28.9	≥ 28.9
Phase error [deg.]	≤ 2.46	≤ 2.52
Excess loss [dB]	0.63	0.68

V. CONCLUSIONS

In this study, we proposed a parallelized structural optimization method based on a real-coded μGA for weakly guided 4×4 MMI couplers for use as optical 90º hybrids. The proposed method was applied to a silica-based 4×4 MMI coupler with $\Delta = 5.5\%$. The optimized 4×4 MMI coupler showed a CMRR greater than 28.9 dBe and a phase error less than 2.52°, which satisfied the typical system requirements over the wavelength range of 1520 to 1580 nm. In addition, the excess loss remained less than 0.68 dB over the wavelength range. The optimization process was executed on a Beowulf-style

cluster comprises five identical PCs. As a result, the speedup and parallel efficiency of the optimization process were 3.90 and 0.78, respectively. A 4×4 MMI coupler with structural parameter values close to the optimized values within an accuracy of typical fabrication tolerance was also analyzed using the FE-BPM. This result is comparable to that of the optimized 4×4 MMI coupler.

ACKNOWLEDGMENT

This work was supported by JSPS KAKENHI (Grant Number JP19K11997). We would like to thank Editage (www.editage.com) for English language editing.

REFERENCES

[1] Y. Sakamaki, Y. Nasu, T. Hashimoto, K. Hattori, T. Saida, and H. Takahashi, "Reduction of phase-difference deviation in 90º optical hybrid over wide wavelength range," *IEICE Electron. Express*, vol. 7, no. 3, pp. 216-221, Feb. 2010.

[2] C. R. Doerr, D. M. Gill, A. H. Gnauck, L. L. Buhl, P. J. Winzer, M. A. Cappuzzo, A. Wong-Foy, E. Y. Chen, and L. T. Gomez, "Monolithic demodulator for 40-Gb/s DQPSK using a star coupler," *J. Lightw. Technol.*, vol. 24, no. 1, pp. 171-174, Jan. 2006.

[3] L. Zimmermann, K. Voigt, G. Winzer, K. Petermann, and C. M. Weinert, "C-band optical 90°-hybrids based on silicon-on-insulator 4×4 waveguide couplers," *IEEE Photon. Technol. Lett.*, vol. 21, no. 3, pp. 143-145, Feb. 2009.

[4] R. Halir, G. Roelkens, A. O.-Monux, and J. G. Wangüemert-Pérez, "High-performance 90º hybrid based on a silicon-on-insulator multimode interference coupler," *Opt. Lett.*, vol. 36, no. 2, pp. 178-180, Jan. 2011.

[5] J. S. Fandino and P. Munoz, "Manufacturing tolerance analysis of an MMI-based 90º optical hybrid for InP integrated coherent receivers," *IEEE Photon. J.*, vol. 5, no. 2, pp. 7900512-7900512, Apr. 2013.

[6] L. B. Soldano and E. C. M. Pennings, "Optical multi-mode interference devices based on self-imaging: Principles and applications," *J. Lightw. Technol.*, vol. 13, no. 4, pp. 615-627, Apr. 1995.

[7] Q. Wang, J. Lu, and S. He, "Optimal design of a multimode interference coupler using a genetic algorithm," *Opt. Commu.*, vol. 209, no. 1, pp. 131-136, Aug. 2002.

[8] B. R. West and S. Honkanen, "MMI devices with weak guiding designed in three dimensions using a genetic algorithm," *Opt. Express*, vol. 12, no. 12, pp. 2716-2722, June 2004.

[9] T. Yasui, J. Sugisaka, and K. Hirayama, "Structural optimization of silica-based 2×2 multimode interference coupler using a real-coded micro-genetic algorithm," *Progress in Electromagnetics Research M*, vol. 55, pp. 169-178, Apr. 2017.

[10] Y. Tsuji and M. Koshiba, "A finite element beam propagation method for strongly guiding and longitudinally varying optical waveguides," *J. Lightw. Technol.*, vol. 14, no. 2, pp. 217-222, Feb. 1996.

[11] T. Yasui, M. Koshiba, and Y. Tsuji, "A wide-angle finite element beam propagation method with perfectly matched layers for nonlinear optical waveguides," *J. Lightw. Technol.*, vol. 17, no. 10, pp. 1909-1915, Oct. 1999.

[12] M. El-Shenawee, C. M. Rappaport, D. Jiang, W. M. Melsei, and D. R. Kaeli, "Electromagnetics computations using the MPI parallel implementation of the steepest descent fast multipole method (SDFMM)," *Applied Computational Electromagnetics Society Journal*, vol. 17, no. 2, pp. 112-122, 2002.

[13] K. Krishnakumar, "Micro-genetic algorithms for stationary and non-stationary function optimization," *Proc. SPIE, Intelligent Control and Adaptive Systems*, vol. 1196, pp. 289-296, Feb. 1990.

[14] C. A. C. Coello and G. T. Pulido, "A micro-genetic algorithm for multiobjective optimization," *Lect. Notes Comput. Sci.*, vol. 1993, pp. 126-140, July 2001.

[15] W. Gropp, R. Thakur, and E. Lusk, *Using MPI-2: Advanced Features of the Message Passing Interface*, 2nd ed., Cambridge, MA, USA: MIT Press, 1999.

[16] L. D. Dalcin, R. R. Paz, P. A. Kler, and A. Cosimo, "Parallel distributed computing using python," *Advances in Water Resources*, vol. 34, no. 9, pp. 1124-1139, Sept. 2011.

[17] F. Herrera, M. Lozano, and J. Verdegay, "Real-coded genetic algorithms: Operators and tools for behavioural analysis," *Artificial Intelligence Review*, vol. 12, pp. 265-319, Aug. 1998.

[18] F. Zhang, K. Sonag, and Y. Fan, "Real-coded genetic algorithm with differential evolution operator for terahertz quasi-optical power divider/ combiner design," *Applied Computational Electromagnetcs Society Journal*, vol. 32, no. 10, pp. 888-894, Oct. 2017.

[19] G. R. Hadley, "Wide-angle beam propagation using Padé approximant operators," *Opt. Lett.*, vol.17, no.20, pp.1426-1428, Oct. 1992.

[20] G. R. Hadley, "Transparent boundary condition for beam propagation," *Opt. Lett.*, vol. 16, no. 9, pp. 624-626, May 1991.

[21] M. Takahashi, Y. Uchida, S. Yamasaki, J. Hasegawa, and T. Yagi, "Compact and low-loss coherent mixer based on high Δ ZrO_2-SiO_2 PLC," *J. Lightw. Technol.*, vol. 32, no. 17, pp. 3081-3088, Sept. 2014.

[22] K. Okamoto, *Fundamentals of Optical Waveguides*, 2nd ed., Cambridge, MA, USA: Academic Press, 2005.

Takashi Yasui graduated with the B.S. degree in Electronic Engineering from Fukui University, Fukui, Japan, in 1997, and the M.S. and Ph.D. degrees in Electronic Engineering from Hokkaido University, Sapporo, Japan, in 1999 and 2001, respectively. From 1999 to 2002, he was a Research Fellow of the Japan Society for the Promotion of Science. In 2002, he joined Fujitsu Ltd., Chiba, Japan. From 2004 to 2011, he was an Assistant Professor of the Department of Electronic and Control Systems Engineering, Shimane University, Matsue, Japan. Since 2011, he has been an Associate Professor of the Faculty of Engineering, Kitami Institute of Technology, Kitami, Japan. He has been engaged in research on wave electronics. Yasui is a member of the IEEE, the Optical Society of America (OSA), the Institute of Electronics, Information and Communication Engineers (IEICE) of Japan, and the Information Processing Society of Japan. In 2018, he was awarded the Excellent Paper Award from IEICE.

Jun-ichiro Sugisaka graduated with the B.E., M.E., and Ph.D. degrees in Optics and Photonics from the University of Tsukuba, Tsukuba, Japan, in 2005, 2007, and 2010, respectively. From 2008 to 2010, he was a research fellow at the Japan Society for the Promotion of Science. From 2010 to 2013, he joined the Center for Optical Research Education at Utsunomiya University, Utsunomiya, Japan, as a doctoral research fellow. From 2013 to 2019, he joined Kitami Institute of Technology as an Assistant Professor. Thenceforth, he has been an Associate Professor of Kitami Institute of Technology. His research interests are in photonic crystals, diffraction, scattering theory inverse problems, artificial intelligence, and computational electromagnetics. Sugisaka is a member of the Institute of Electronics, Information and Communication Engineers (IEICE) of Japan, the Japan Society of Applied Physics, IEEE, and the Optical Society of America. In 2018, he was awarded the Best Paper Award from the IEICE.

Koichi Hirayama received the B.S., M.S. and Ph.D. degrees in Electronic Engineering from Hokkaido University, Sapporo, Japan, in 1984, 1986 and 1989, respectively. In 1989, he joined the Department of Electronic Engineering, Kushiro National College of Technology, Kushiro, Japan. In 1992, he became an Associate Professor of Electronic Engineering at Kitami Institute of Technology, Kitami, Japan, and in 2004 he became a Professor. He has been interested in the analysis and optimal design of electromagnetic and optical waveguides. Hirayama is a senior member of IEEE. In 2018, he was awarded the Excellent Paper Award from IEICE.